

ACOUSTIC LINER DESIGN FOR FENESTRON® NOISE REDUCTION

Reinhard Pongratz

reinhard.pongratz@airbus.com

Daniel Redmann

daniel.redmann@airbus.com

Airbus Group Innovations
Taufkirchen, Germany

Abstract

The paper presents work done on the design of two different liners for FENESTRON® noise reduction on a 0.7:1 scaled H135 test rig. A short presentation of typical H135 spectral noise emission is given which forms the basis for the liner design regarding its spectral absorption domain. The existing H135 test rig is described, the modification according to the BLUECOP-TER™ design of Airbus Helicopters as shroud design, stator design and fan blade design are presented. After describing test procedure and test parameter the design of the liner is given. According to tonal BPF noise components resulting from turbulent inflow conditions and rotor stator interaction and stochastic broadband components due to high vorticity flow at the fan blade tips two kind of liner haven been designed. An acoustic, double degree of freedom (DDOF) liner was studied both, numerically and by experiments and integrated behind the fan plane. His absorption efficiency was simulated and tested. In addition an aerodynamic liner was integrated for vorticity reduction in the vicinity of the fan blade tips by allowing flow penetration into a partially permeable shroud surface. Stochastic noise reduction was expected due to vorticity reduction. The efficiency of both types of liner could be demonstrated by measurements. Up to 3 dB(A) OASPL reduction was demonstrated.

1. INTRODUCTION

Helicopters often operate in the neighbourhood of urban areas requiring modern eco-friendly aircraft. Due to population acceptance along with tightened noise certification regulations manufacturer are forced for improved low noise solutions. Major helicopter noise sources are main rotor, tail rotor and engine depending on flight conditions as approach, take-off, level flight or hover. Regarding rotational noise sources main and tail rotor are predominant. During the past much effort have been done to develop main rotor noise source reduction technologies and large progress could be achieved. Examples are low noise blade design as the

BlueEdge™ blade from Airbus Helicopters, (AH), with modified blade tip, or the individual blade control technique by trailing edge flaps, reduced tip speed design or modulated blade spacing. As main rotor noise is reduced tail rotor noise becomes more discernible within the overall noise emission. Regarding further helicopter noise reduction measures tail rotor noise must not be neglected. For usual tail rotors many of the methods developed for main rotors are also possible noise reduction measures. However, some mid and light-weight helicopter models are equipped with shrouded tail rotors, so called FENESTRON®. Besides improved operational safety near ground and advanced performance efficiency, the FENESTRON® offers

substantial acoustic benefits in contrast to the open tail rotor [1], [2]. Whereas previous and actual work of Airbus Helicopters concentrate on direct noise reduction measures, (modulated blade spacing, non-radial stator blades, reduced number of stator blades, optimized blade planform design), this paper documents indirect noise reduction methods using liner technologies for noise absorption and noise prevention. Hereby the potential advantage of the FENESTRON® shroud was used for liner integration. The experimental work described have been done on a 0.7:1 scaled model of the H135 FENESTRON® as available at the aeroacoustic laboratory of Airbus Group Innovations.

2. H135 FENESTRON® NOISE EMISSION

Despite the already low noise emissions of the H135 FENESTRON® there are some flight conditions at which its noise characteristic determines the perceived noise at ground. In particular this happens at high blade loads during hover or at special yaw angles leading to bad flow conditions on the blades. At those conditions strong tonal noise components are emitted dominating the psycho-acoustic noise characteristics. A typical spectral noise emission characteristic at adverse flow conditions during approach is given in the diagram of Fig. 1. Harmonic components of the FENESTRON® tones are marked.

Due to the modulated spacing of the ten FENESTRON® blades the noise emission is dominated by tones of frequencies according to $2 \cdot \text{rpm}$ and its harmonics. The higher harmonic components are within the frequency range of 500 Hz to 1.5 kHz. At these frequencies the human ear is relative sensitive resulting in annoying noise sensation.

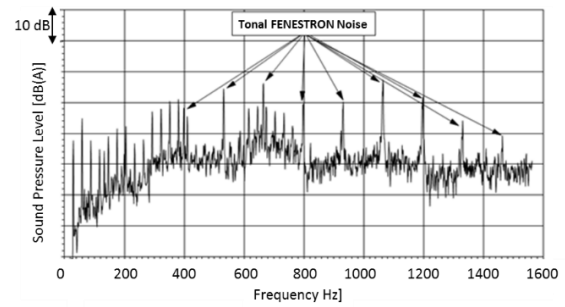


Fig. 1: H135 spectral noise emission during approach (Source: Airbus Helicopters)

Fig. 2 shows the noise emission situation at main rotor retreating side during hover. Again, the FENESTRON® noise harmonics are indicated. Especially within a frequency range around 1 kHz these tones emerge from the broadband noise floor indicating that they are clear audible.

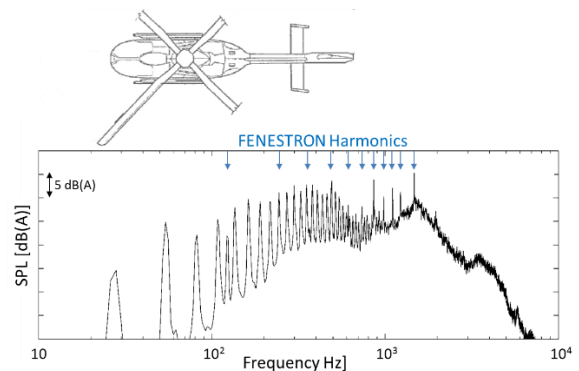


Fig. 2: H135 spectral noise emission to retreating blade side at hover (Source: Airbus Helicopters)

The higher harmonic components are within the frequency range of 500 Hz to 1.5 kHz. At these frequencies the human ear is relative sensitive resulting in annoying noise sensation. Thus, the liner tuning should ensure a good sound absorption already at a lower frequency bound of about 500 Hz. Fig. 2 indicates also relevant broadband noise emissions in the frequency range above 1.5 kHz. The liner should therefore be able to offer good absorption at this higher frequency range.

3. TEST RIG DESCRIPTION

For the tests a 0.7:1 scaled EC153 FENESTRON® model was used which is available at the AGI acoustic lab. The FENESTRON® casing is mounted on an adjusted support which itself is fixed to the rig bearing the motor and the drive shaft. The drive shaft itself is driven by a 37.5 kW electro motor via a belt transmission. The actual rig configuration allowed a maximum rotation speed of 4730 rpm corresponding to a maximum blade tip Mach number of 0.50 at a blade pitch angle of 25°. The maximum rotational speed depends on the blade pitch angle and is limited by the maximum electric power of the motor and the frequency converter driving the motor.

For the blade fixation two new hubs was manufactured with a diameter of 266 mm resulting in an $\varnothing_{\text{hub}}/\varnothing_{\text{shroud}}$ ratio of 0.38. One hub allows an equidistant arrangement of the 10 rotor blades, whereas the second hub enables a modulated blade spacing. Within this paper only test results with the unevenly spaced blades are given.

The stator configuration is according to the new stator on the AH BLUECOPTER™ which uses only two curved stator vanes in addition with the geometric dominant drive shaft fairing. The two blades are arranged non-radial with varying angles in-between and with the drive shaft fairing.

The fan blades used represent the new fan blade design of as implemented on the AH BLUECOPTER™. A photograph of the test rig is given in Fig. 3.

A some more detailed view to the design of the scaled shrouded fan is given in the drawings of Fig. 4. Again the shroud contour are identical to the BLUECOPTER™ design.



Fig. 3: 0.7:1 scaled FENESTRON® test rig with unevenly spaced 10-bladed rotor, 2-bladed curved stator and drive shaft fairing

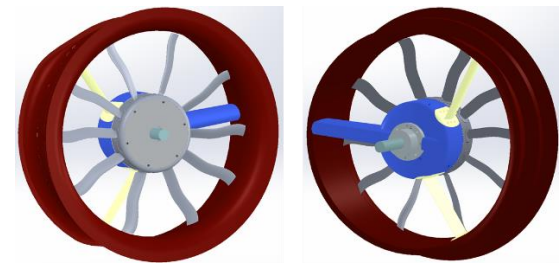


Fig. 4: Front and rear view of the shrouded fan

In order to get comparable acoustic results the knowledge about the actual thrust delivery for every configuration is essential. Therefore the thrust was measured during each measurement. To enable this measurement the whole test rig was mounted on four sliders which can traverse on two tracks, Fig. 5. This allows the rig to move free and with low friction in the direction of the rotor-axis.

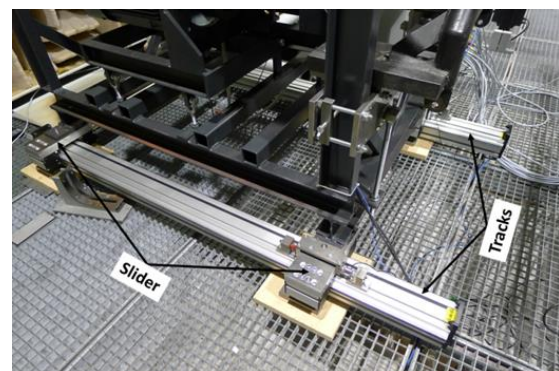


Fig. 5: Loosely rig mounting on two tracks

Thrust was measured by two load cells which have been mounted on both tracks. Therefor the load cells were clamped between a slider and a clamping pedestal. To overcome the static friction a pretension was applied on both sides by two spiral springs as shown in Fig. 6

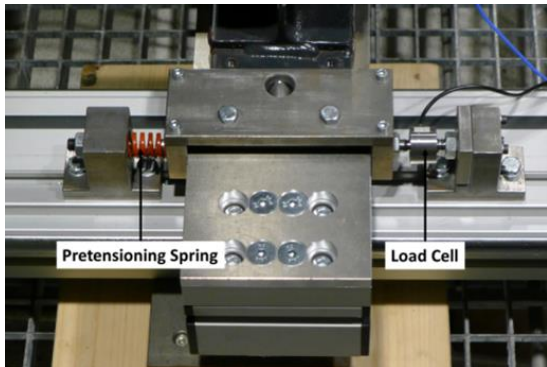


Fig. 6: Load cell integration for thrust measurements

The thrust measurements have been calibrated using known weights between 0.8 kg and 14 kg which have been attached to the rotor shaft. The resulting calibration curve is given in the diagram of Fig. 7. This diagram comprises the calibration results done at 6 different days. Besides a small tendency to measure a somewhat, ($\approx 2.6\%$), higher weight compared to the reference value the calibration results are very well reproducible.

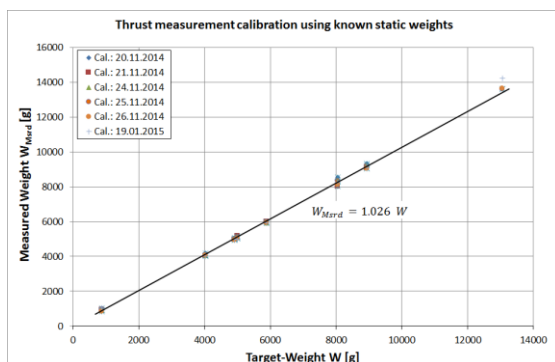


Fig. 7: Thrust measurement calibration curve

4. LINER DESIGN

In order to reduce the noise emitted into the far-field two different lining concepts have been designed and integrated:

- Two degree of freedom acoustic liner integrated at the pressure side of the shroud, just behind the rotor plane.
- Aerodynamic blade tip liner integrated into the shroud and located within the rotor plane.

The aerodynamic blade tip liner was chosen to reduce broadband tip clearance noise by offering the tip clearance flow a permeable surface. Due to flow penetration into this permeable surface vorticity will be reduced resulting in lower values for the turbulent kinetic energy and therefore reducing the acoustic source strength.

4.1. Acoustic Liner

Design goal for the acoustic liner was to ensure good sound absorption within a wide frequency range. Furthermore the liner should ensure a good sound absorption already at a lower frequency bound of about 500 Hz. Using an in-house code for the dimensioning of a new, 2 degree of freedom liner, known as slot absorber, the liner geometry was determined and the expected sound absorption have been estimated. The idea of this new design follows the Special Acoustic Absorber concept, which combines a Helmholtz Resonator absorbing sound in the lower frequency range and a $\lambda/4$ -Resonator for noise reduction at the mid and higher frequencies. However, the new slot absorber concept uses a simplified design which is easier to manufacture, especially in case of curved structures. The inner structure of this new liner is given in Fig. 8.

The integration of this two degree of freedom liner into the FENESTRON® shroud is given in Fig. 9.

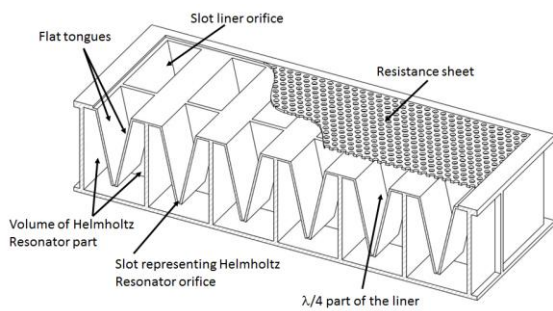


Fig. 8: Inner structure of the new slot-liner quoted for the example of a flat sample

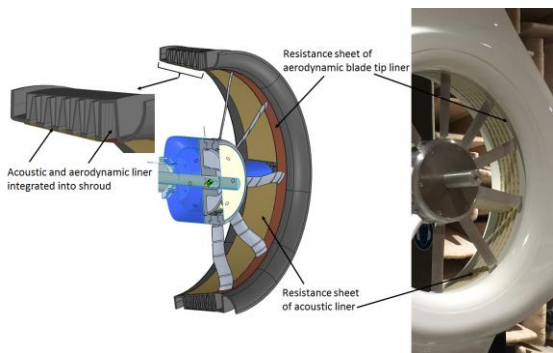


Fig. 9: Integration of acoustic and aerodynamic liner into the shroud

Within the diffuser part of the shroud 5 rows of annular arranged single slot absorbers are integrated. In order to enlarge the absorption bandwidth of the whole liner arrangement further the total depths of the slot absorber elements differs slightly from ring to ring according to the diffuser cone angle. The maximum volume depth of the absorber elements located just behind the rotor is 51 mm, the minimum depth of the absorber elements near the diffuser exit is 36 mm. Each of the five liner rings contains 80 single slot absorber elements. At the end 400 single absorber elements have been integrated into the liner.

One drawback of this design is the insufficient usage of the available absorption area of the liner. In case of the integrated FENESTRON® liner only about 40% of the available surface are used for sound absorption. However, this design was a very first one. In the meanwhile the design was

improved such that the available sound absorption area is above 90%. This could be achieved by replacing the flat tongues with curved ones, Fig. 10. The frequency ranges at which the liner works is affected only minor.

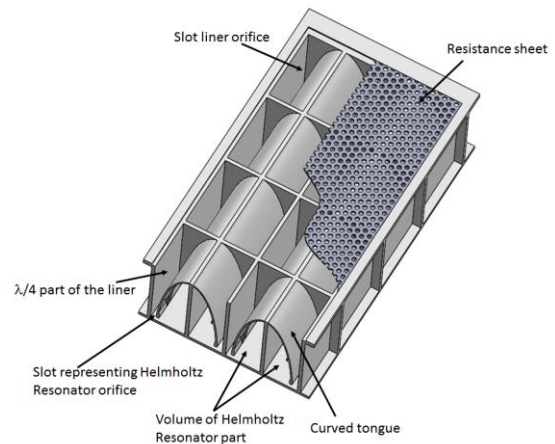


Fig. 10: Advanced slot liner design offering maximum sound absorption area

For the flat sample design as given in Fig. 8 the insertion loss was numerically simulated, (full 3D), and also measured within a rectangular flow duct owing a cross sectional area of 100 x 70 mm². The numerical model is given in Fig. 10, both results are given in the diagram of Fig. 11. In the lower frequency range the measurement result is reproduced well by the numeric simulation. At higher frequencies the simulation forecasts a higher transmission loss which might due to wave reflections inside the channel which are not accounted for by the analyzing procedure.

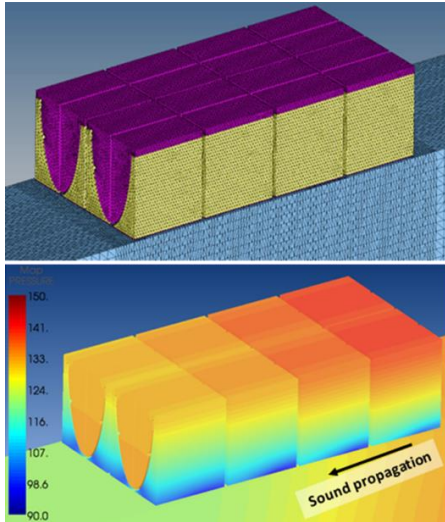


Fig. 11: Slot liner flat sample within flow tube: Mesh model, top, and sound pressure level distribution at 660 Hz, bottom

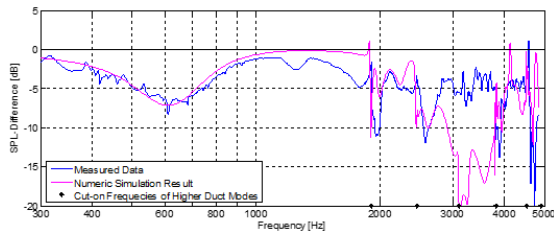


Fig. 12: Measured and simulated transmission loss of slot liner flat sample as shown in Fig. 7 within flow duct

As resistance sheet a 2-layer stainless steel compound weave of type TM2KT10 was used. This wire mesh offers an almost constant acoustic resistance of 1.4 ρc over the whole frequency range. However, the optimum impedance of an acoustic liner depends on frequency, mode, flow velocity, sound pressure level and other conditions. The resistance value of 1.4 ρc , as chosen for the wire mesh used may be a good compromise for the whole frequency range between 500 Hz and 2 kHz. However if the lower frequencies are focused a slightly lower resistance would have been a better choice.

Using a small mobile impedance tube, (\varnothing 29 mm), the surface impedance for normal sound incidence was measured at several positions of the liner integrated into the shroud. The measured mean impedance

values and standard deviations are plotted in the two diagrams of Fig. 13. The results confirm the Helmholtz resonance at about 650 Hz together with a resistance of about 1.4 ρc . The anti-resonance of the DDOF slot liner is at 1750 Hz, owing high impedance there and minimizes the sound absorption in this frequency range. The $\lambda/4$ -resonance is at about 2350 Hz. In this frequency range the liner resistance is at about 2 ρc .

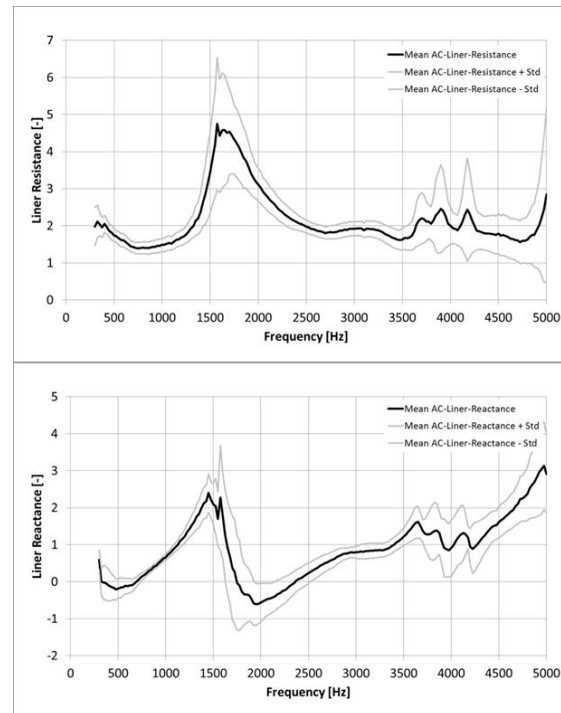


Fig. 13: Measured mean surface impedance, (resistance and reactance), of the integrated liner for normal sound incidence

4.2. Aerodynamic Liner

The idea of the blade tip liner is to reduce the vorticity within the tip clearance flow and therefore to reduce the acoustic source strength of broadband noise which is produced there, especially at high FENESTRON[®] power settings. In case of the FENESTRON[®] test rig the gap width of the tip clearance is 3 mm, Fig. 14, which gives a value for the relative gap height τ defined as relation between gap and rotor diameter of $\tau = 0.0043$.



Fig. 14: Tip clearance at the scaled FENESTRON® test rig

Kameier, [3] states in his work that, in case of a high pressure compressors, tip clearance noise becomes relevant at relative gap beyond $\tau = 0.0027$. With decreasing gap width tip-clearance noise reduces significantly. He identified a rotating source mechanism, called rotating instability, moving relative to the blade row at a fraction of shaft speed.

Khorrami et al., [4], identified two mechanisms responsible for tip clearance noise. One is due to the unsteady flow field in the tip vicinity interacting with the tip surface and producing self-generated broadband noise. The second mechanism is due to the down-stream convection of the tip vortex interacting then with the stator vanes leading to mainly tonal noise. They addressed porous treatment as effective measure for tip-vortex intensity reduction and weakening a dominant component of rotor self-noise.

Sutliff et al., [5], integrated a foam-metal liner in close proximity to the rotor by which fan noise could be reduced up to 4 dB.

Within this work the reduction of vorticity will be achieved by offering a flow permeable shroud surface within the rotor plane. This can be realized by introducing a circumferential u-shaped channel within the shroud which is covered by a wire-mesh.

This channel is 28 mm wide, (in flow direction), and is 52 mm deep.

The modelling of the noise reduction physics is not reliable possible with the tools available because both, the turbulent tip clearance flow as well as the turbulent flow through the wire mesh surface must be modelled in full 3D at very fine temporal and spatial resolutions in order to allow the extraction of the acoustic relevant pressure fluctuations. The necessary CFD amount was beyond the scope of the project.

The difficulty is to find the optimum resistance of the permeable surface. In contrary to the acoustic liner does the blade tip liner not primarily absorb the acoustic energy, which needs resistance values around 1 pc . Here the vorticity within the 3 mm wide tip clearance flow should be reduced and therefore the turbulent flow must be able to penetrate into the shroud surface. This means that the surface resistance must be not too high. Fig. 15 gives acoustic resistance values for different types of 2-layer stainless steel compound weaves as measured within an impedance tube. The resistance values are plotted against Euler's Number, given by the mesh manufacturer. Euler's Number represents a dimensionless number in flows and indicates the ratio between pressure and inertia forces.

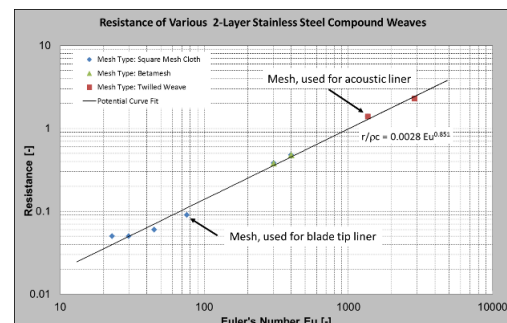


Fig. 15: Measured acoustic resistances of various 2-layer stainless steel compound weaves

The author decided on the mesh type TM2BM50 which offers an acoustic resistance of 0.09 pc. The complete liner integration is shown schematically in the CAD plot of Fig. 16

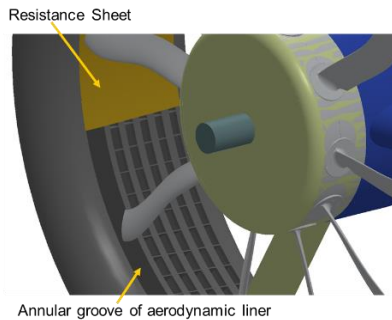


Fig. 16: CAD plot of aerodynamic and acoustic liner integration

Finally covered blade tip liner and acoustic liner integration into the test rig is shown in the photograph of Fig. 17.

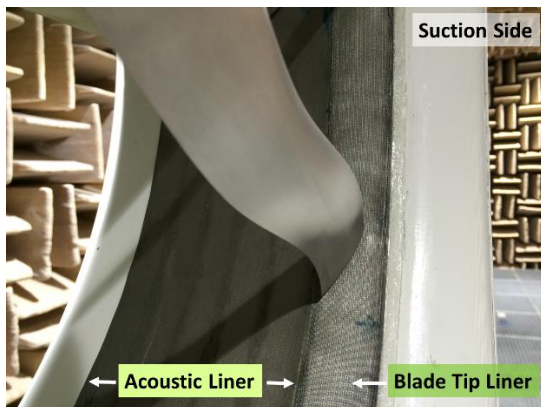


Fig. 17: View on the aerodynamic blade tip liner (blade pitch angle: 25°)

5. RESULTS

This chapter presents numerical simulation results, describe the experimental test procedure and demonstrates the measured noise reductions achieved.

5.1. Numerical Simulations

For the scaled test rig a full 3D-numerical model was meshed using Hypermesh, Fig. 18. The liner geometry was therefore also fully dissolved in 3D allowing a realistic simulation of its acoustic reactance.

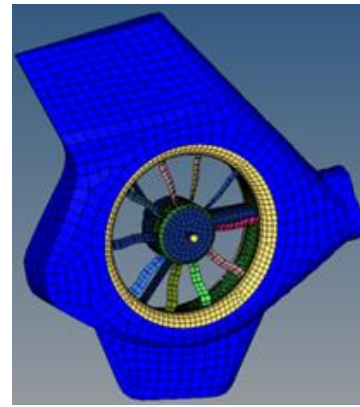


Fig. 18: Full 3-D Hypermesh model of the scaled test rig

The liner resistance was simulated by defining a surface resistance corresponding to the measured values of the wire mesh. All acoustic simulations have been done in frequency domain by using the commercial tool ACTRAN-TM. The corresponding model is given in Fig. 19

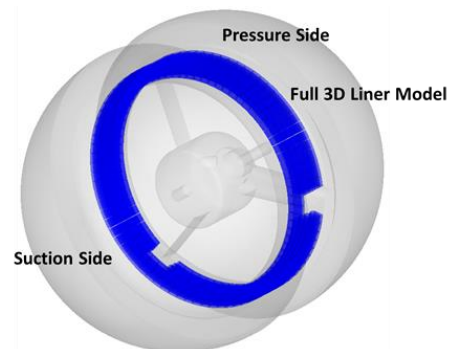


Fig. 19: ACTRAN-TM model for numerical noise simulations.

For noise excitation 10 artificial monopoles have been positioned within the fan plan at 70% rotor radius. All simulations have been done using tonal excitation at the 1/3rd-octave mid-frequencies. Due to missing relevant flow data the simulation were done without flow. A typical resulting intensity distribution on the suction side positioned hemisphere is given in Fig. 20 for the two frequencies of 630 Hz and 2500 Hz. Under the simulation boundary conditions the simulated noise emission is as expected, the main directivity is on the fan axis. At

higher frequencies modal pattern are visible within the fan duct.

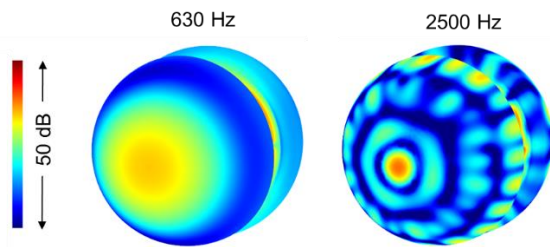


Fig. 20: Simulated intensity distribution on suction side located hemisphere for 630 Hz and 2500 Hz.

The effect of the liner is given on pressure distribution inside cut-planes within the shrouded fan for side and front view as given in Fig. 21. The effect of the liner is clear visible. Looking at the side view cut-plane one can see that the liner reduces the sound pressure within the fan duct. Furthermore, the noise emission to the pressure side of the FENESTRON® is also considerably reduced.

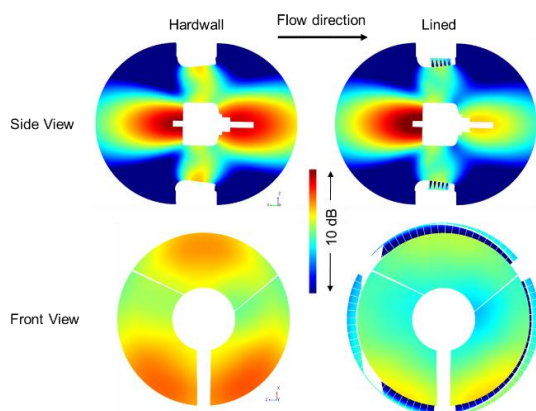


Fig. 21: Simulated sound pressure distribution inside two cut-planes, side and front, (suction-side), view for hardwall and lined condition at 630 Hz. (Flow from left to right)

The front side view shows that at this low frequency a pressure pattern according to the 1st tangential mode order develops with pressure maxima in the vicinity of the drive shaft fairing. The liner is able to reduce the sound pressure remarkably over the whole duct radius.

Fig. 22 gives the same pressure distribution for a frequency of 2500 Hz. Again, noise is

well reduced near the liner surface and for pressure side emission. At this frequency the pressure pattern within the front view duct-plane is governed by the 10 artificial monopole noise sources.

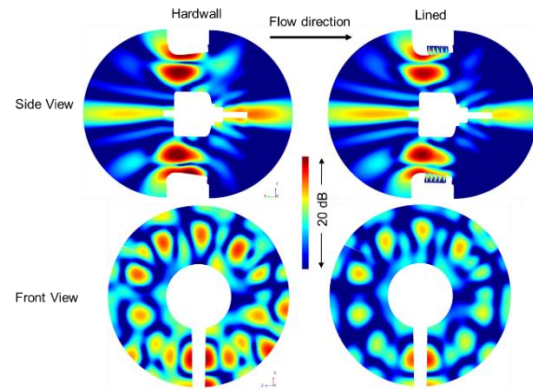


Fig. 22: Simulated sound pressure distribution inside two cut-planes, side and front, (suction-side), view for hardwall and lined condition at 2500 Hz. (Flow from left to right)

As the acoustic liner is located in flow direction behind the fan plane a remarkable effect on suction side cannot be observed and could also not be expected.

For pressure side noise emission the spectral liner efficiency is given over the simulated frequency range in the diagram of Fig. 23. There the sound pressure levels averaged over the hemisphere surface are plotted for hardwall and lined condition. The two absorbing frequency ranges of the double degree of freedom liner are clear visible around 630 Hz and around 2500 Hz. In-between the anti-resonance prohibits sound absorption due to high impedance. This simulated spectral absorption result confirms well to the measured spectral liner impedance given in Fig. 13.

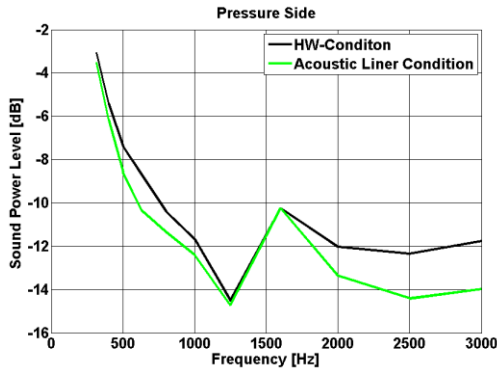


Fig. 23: Simulated mean spectral noise reduction averaged over the pressure side hemisphere

5.2. Test Procedure

All tests have been done within the anechoic room of the acoustic laboratory of AGI. For the measurements the suction side of the FENESTRON® was oriented into the room while the pressure side pushes the air outwards as shown in Fig. 24. However, due to this operating condition poor flow conditions must be assumed. The air sucked outside through the large door must be balanced by an inside floor also through the same door. Therefore an annular flow condition must be supposed. As only comparative measurements are done these poor flow conditions should not affect results regarding liner efficiency too much.

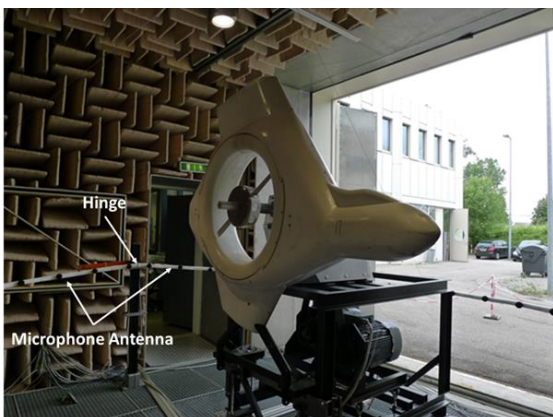


Fig. 24: Rig orientation during the measurements within the anechoic room

All measurements have been done using a ramp-like rpm profile for the rotor acceleration and deceleration and a stationary phase in-between with maximum rotor speed. For each of these three phases a time of about 60 s was chosen resulting in a typical cycle time of about 180 seconds. This paper concentrates on the analysis during maximum constant rpm. For the different configurations tested the maximum constant rpm showed variations between 4650 and 4730 rpm.

Fig. 25 gives second order fit results to all measured thrust values for each of the four liner configurations during up- and down-ramping. In addition one typical thrust measurement curve is plotted showing hysteresis behavior typical for the thrust measurement on the test rig. At each measurement the thrust during down-ramping was always higher in comparison with the up-ramping phase. One reason may be due to additional acceleration work done by the rotor during ramp up. In addition different warping of the sliders on the two tracks during acceleration and deceleration may also influence the thrust measurement leading to different results during ramp-up and ramp-down. At maximum drive the rotor delivers a thrust of about 110 kg.

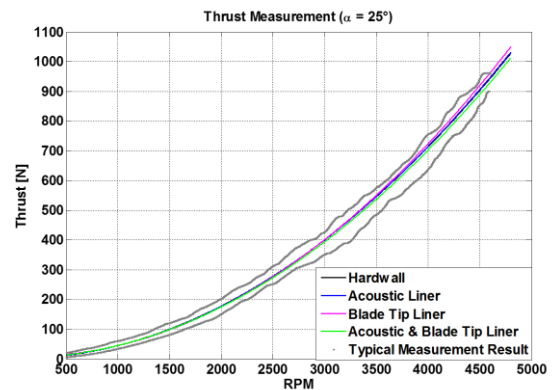


Fig. 25: Fitted thrust data versus rotor rpm for all liner configurations during up and down ramping

5.3. Noise Reduction

For the noise measurements different rig configurations was defined:

- Hardwall configuration
- Only acoustic lining behind rotor plane active
- Only aerodynamic lining in rotor plane active
- Acoustic and aerodynamic lining active

For the acoustic measurements 2x19 microphones have been mounted on two semi-circular arcs. These two arcs are able to pivot around a common hinge and scan the upper hemisphere of the test-rig. The arcs diameters are 4 m. The hinge of the arcs is within the rotor plane and 65 cm below the rotor axis, Fig. 24. The distance of the microphones on the two arcs is according to 10° . The type of the free-field condenser microphones used are Class1 constant current powered $\frac{1}{4}$ " electret measuring microphones M360 from Microtech Gefell. They offer a nominal sensitivity of 12.5 mV/Pa over a frequency range of 20 Hz – 20 kHz. All microphones were calibrated and covered by a windscreen. As data acquisition unit the Scadas-X system from LMS was used allowing a synchronous acquisition of all measured microphone, thrust and rpm signals. Each channel have been sampled using a sampling rate of 20480 Hz

- Hardwall Condition

Hardwall condition was achieved by covering the mesh surfaces with aluminum tapes. These tapes block the noise transfer through the meshes and offer a smooth surface.

For hardwall condition the mean, spatially averaged A-weighted sound power spectra emitted to pressure respectively suction side at constant maximum rpm, (rpm = 4690) are given in the two diagrams of Fig.

26. The spectra are dominated by the BPF-harmonics, starting at 8 BPF. According to the 10 blades the maximum noise emission is at 10 BPF for both sides of the FENESTRON®. Due to the symmetric structure of the unevenly spaced fan blades the spectra are dominated by even BPF-multiples. On pressure side the mean over all sound pressure level (OASPL) is 108.5 dB(A), on suction side 107.8 dB(A). As expected, the main acoustic energy is tonal and within the frequency interval from 500 Hz up to 2 kHz.

In order to distinguish between the tonal components from the remaining broadband noise the tones have been extracted in time domain using the in-house code ROSI. This enables estimation of the liner effect on the tones and on broadband noise components.

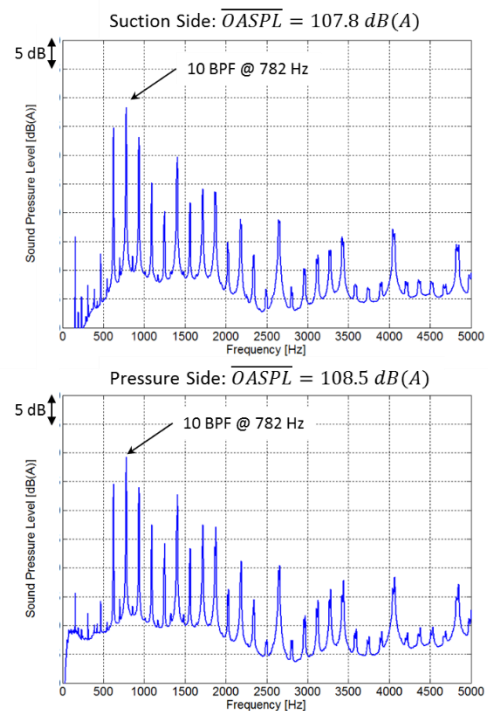


Fig. 26: Emitted sound power spectra on suction and pressure side, spatially averaged over the corresponding hemisphere for hardwall condition (GHD-blades at 25° pitch angle)

The remaining broadband component was calculated for each microphone and antenna position by the subtraction of the tonal signal from the original measured ones.

The results are presented for suction side in the diagram of Fig. 27. Within the extracted tonal noise spectrum a higher signal dynamic can be recognized. Now all rpm-harmonics are visible.

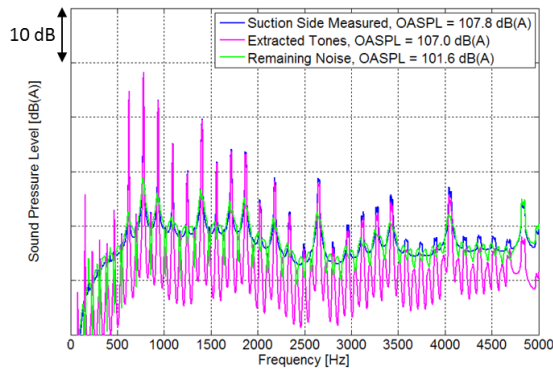


Fig. 27: Comparison between measured power spectra and the spectra for the extracted tones only (suction side)

The emitted over-all sound pressure level distribution on the measured hemisphere around the test rig are given in Fig. 28. Higher noise levels are emitted to pressure side and the noise emission directs mainly to the upper side of the rig on both, suction and pressure side.

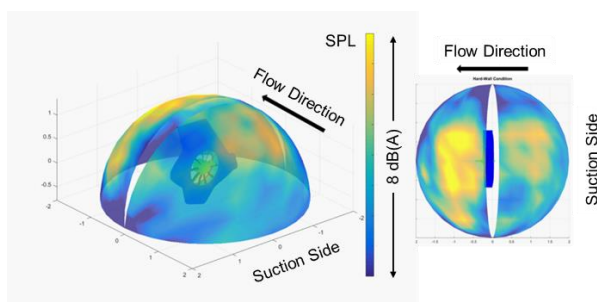


Fig. 28: Measured surface sound pressure level on the hemisphere around the test rig at hardwall condition

Tonal noise emission characteristic for the 10th BPF harmonic at 782 Hz and the 36th BPF harmonic at 2815 Hz are plotted in Fig. 29. For this isolated tones an emission characteristic typical for duct noise becomes visible, especially for the 36th harmonic. The noise emits mainly cone like resulting in a ring like structure of the SPL on

the hemisphere. On the fan axis minimum noise emission is observed.

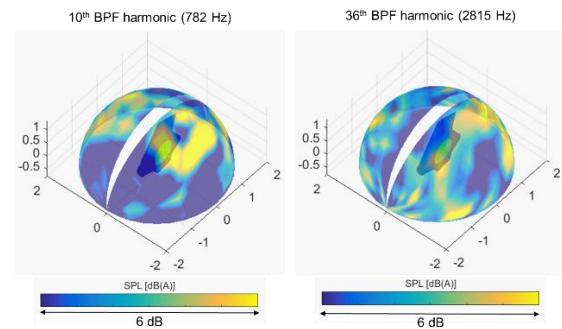


Fig. 29: Noise emission characteristic for the 10th and 36th BPF harmonic under hardwall condition

- Lined Condition

An overview about the noise reduction achieved for all tested conditions is given in the diagram of Fig. 30. This diagram compares the mean sound pressure levels on the measured hemisphere surfaces at intake and exhaust. The noise levels have been calculated for

- all spectral components (OASPL)
- all BPF-harmonics
- the dominant BPF-harmonics only (9.–11. Harm. = 600-1000 Hz)
- the high frequency harmonics (34.–56. Harm = 2500-4200 Hz)

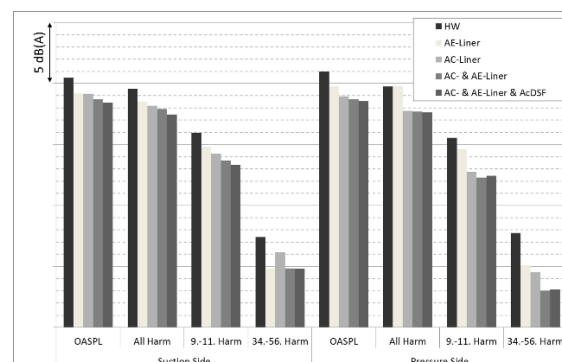


Fig. 30: Comparison of liner condition on mean over-all and tonal sound pressure level at suction and pressure side as measured.

The two frequency ranges, (9.–11. and 34.–56. BPF harmonics), have been chosen as the two degree of freedom slot liner has its

maximum absorption within these two intervals.

Using the acoustic liner only 2.5-3 dB(A) noise reduction was achieved within its two absorbing frequency ranges on pressure side. At intake the tone levels have still been reduced by 1–1.5 dB(A) although the liner is located behind the rotor.

The aerodynamic blade tip liner alone delivers a slight reduction at the lower BPF-harmonics, similar on both sides of the test rig. Up to 2 dB(A) noise reduction could be measured in the higher frequency ranges on both sides of the rotor.

Combining both liner a tonal noise reduction of 2.5 dB(A) on suction side and of 3-4.5 dB(A) on pressure side could be achieved within these two frequency ranges. The over-all sound pressure levels reduce by 2 dB(A) at intake and 2.5 dB(A) at exhaust.

Besides the liner efficiency the acoustic relevance of the drive shaft fairing could be demonstrated. The last bars for each spectral interval show the SPL's when the drive shaft fairing and the two stator blades are removed. A considerable noise reduction could be measured, especially at the dominating 9th to 11th BPF-harmonics. On suction side the SPL reduces by 8.5 dB(A) and by 6.5 dB(A) at exhaust at these frequencies. An over-all a noise reduction potential of 4.2(A) at intake and 3.8 dB(A) at exhaust could be demonstrated.

If one corrects for the small rpm variations between the different tests, which are in the interval [4678 ... 4733], for a constant rpm corresponding to a thrust of 1 kN SPL-differences to hardwall configuration can be found as given in the diagram of Fig. 31. In this diagram dominates the large noise reduction potential when the drive shaft fairing is removed, especially for the BPF tones. The above mentioned noise reduc-

tion potential of the aerodynamic liner especially at higher frequencies is confirmed. On the tones at lower frequencies this liner has only marginal effect whereas the acoustic liner shows a good efficiency within a range which could be expected from the simulation results.

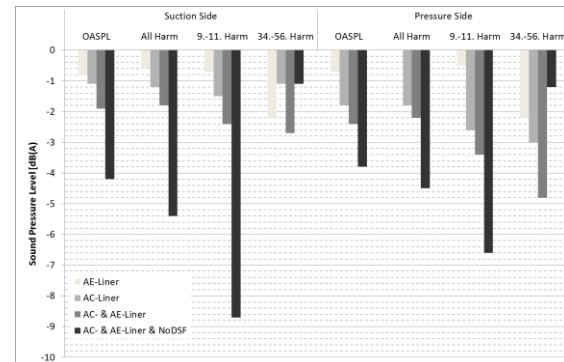


Fig. 31: Thrust-corrected SPL-reductions for the various liner configurations on different spectral components

If one distinguish between tonal and broadband noise reduction results as shown in Fig. 32 are produced. This diagram confirms that the aerodynamic liner is most effective for the broadband stochastic noise components. This liner delivers only marginal tone noise reductions. The acoustic liner reduces the tone noise levels and also broadband components especially on pressure side. This higher noise reduction on pressure side results from its location behind the fan plane.

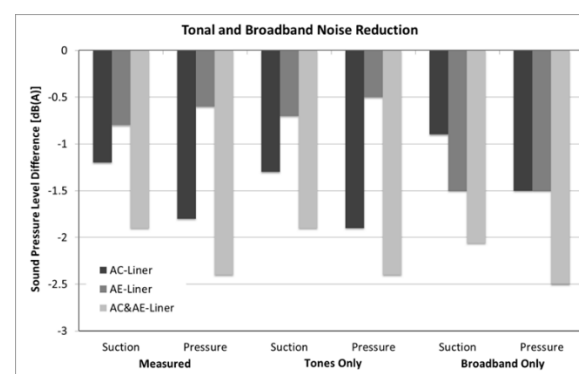


Fig. 32: Measured over-all tonal and broadband sound pressure level reductions on suction and pressure sides for acoustic and aerodynamic liner configuration

Finally a comparison between measured and simulated noise reduction at 1/3-octave mid frequencies is given in Fig. 33. Both, simulation and measurement results confirm very well, the acoustic liner was working as could be expected due to its design considerations.

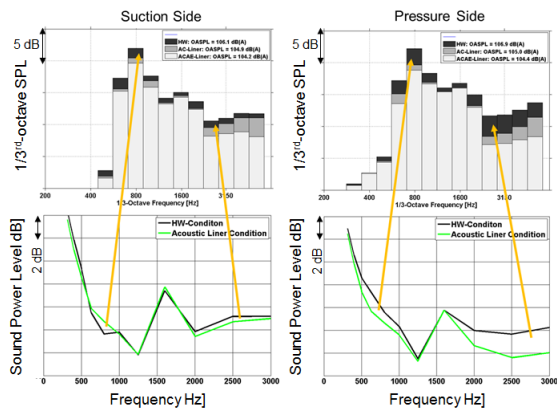


Fig. 33: Comparison between measured and simulated noise reduction at suction and pressure size

For the 70%-scaled FENESTRON® test rig with its short fan duct, $L/D \approx 0.25$, an overall noise reduction of 2.5 dB(A) could be simulated and measured. Not shown here, the annoyance of the emitted noise could also be reduced due to the broadband depression of the sound pressure levels in the higher frequency range. The effect of the liner clearly audible.

Flight tests done with integrated aerodynamic and acoustic liner demonstrated a remarkable tonal and broadband noise reduction on the AH Green Helicopter Demonstrator BLUECOPTER™. Detailed information are given in Ref. [6] and therefore not further discussed in this paper.

6. SUMMARY AND OUTLOOK

In order to document the efficiency of various FENESTRON® noise reduction measures tests on the 0.7:1 scaled H135 FENESTRON® test rig have been designed and done at the acoustic laboratory of AGI. These measures comprise different rotor

blade de-sign, acoustic and hydrodynamic liner integration into the shroud and an acoustically treated leading edge of the drive shaft fairing. All tests have been done without external approaching flow. During all noise measurements the shaft drives as well as the thrust were recorded together with microphone measurements on a hemisphere like surface around the test rig.

This report documents the noise reduction potential at suction and pressure sides of the test rig due to acoustic liner integration behind the rotor and aerodynamic blade tip liner integration within the rotor plane.

The tests confirmed an over-all noise reduction potential of 2 to 2.5 dB(A) due to the combined liner. For the dominating tonal BPF-harmonics a noise reduction potential of 2.5 to 3 dB(A) could be demonstrated.

Removing the drive shaft fairing the emitted noise reduces by 4 dB(A) over-all.

The simulations described here are done without flow and non-rotating fan. Future numerical work should include first a flow field as produced by the rotating fan. This can in a first step be a stationary RANS calculated field. In a second step flow data from non-stationary CFD calculations should be integrated. A comparison between both results would be interesting. Also flow effects on the liner absorption as well as on the noise emission to the far-field should be studied.

In case of experimental work measurements on the lined test-rig within a representative wind tunnel would be very advantageous.

ACKNOWLEDGEMENTS

The activities on acoustic liner design for FENESTRON® noise reduction have been possible due to in-house funding and the support of the topic by Airbus Helicopter. The fundamentals of the acoustic liner adapted to FENESTRON® conditions are developed within the German aeronautical research program LuFo IV as funded by the Federal Ministry of Economics (BMWi) in the project LeiLa.

REFERENCES:

- [1] Niesl, G. and Arnaud, G., "Low Noise Design of the EC 135 Helicopter", American Helicopter Society, 52nd Annual Forum, Washington, D.C., United States, June 4-6, 1996.
- [2] M. Roger, "Applied Aeroacoustic Methods for the Acoustic Design of a Shrouded Tail Rotor", CEAS/AIAA-95-137
- [3] Kameier F., „Experimentelle Untersuchung zur Entstehung und Minderung des Blattspitzen-Wirbellärms axialer Strömungsmaschinen“, Hermann-Föttinger-Institut für Thermo- und Fluid-dynamik Technische Universität Berlin, 1993
- [4] Khorrami M.R., Li. F, Choudhari M., „A novel approach for reducing rotor tip-clearance induced noise in turbofan engines“, AIAA-2001-2148
- [5] Sutliff D.L., Jones M.G., "Low-Speed Fan Noise Attenuation from a Foam-Metal Liner", Journal of Aircraft, DOI: 10.2514/1.41369, Paper 2897, E-18267, 2011
- [6] Schneider S., Heger R., Konstanzer P., „Bluecopter™ Demonstrator: The State-of-the-Art in Low Noise Design“, European Rotorcraft Forum 42nd, Lille, France, September 2016

Copyright Statement

The authors confirm that they, and/or their company or organization, hold copyright on all of the original material included in this paper. The authors also confirm that they have obtained permission, from the copyright holder of any third party material included in this paper, to publish it as part of their paper. The authors confirm that they give permission, or have obtained permission from the copyright holder of this paper, for the publication and distribution of this paper as part of the ERF proceedings or as individual offprints from the proceedings and for inclusion in a freely accessible web-based repository.